PCCP

PAPER

View Article Online
View Journal | View Issue

Cite this: *Phys. Chem. Chem. Phys.*, 2023, **25**, 26278

A systematic mid-infrared spectroscopic study of thermally processed SO_2 ices

Duncan V. Mifsud, *[ab] Péter Herczku, [b] K. K. Rahul, [b] Ragav Ramachandran, [c] Pavithraa Sundararajan, [c] Sándor T. S. Kovács, [b] Béla Sulik, [b] Zoltán Juhász, [b] Richárd Rácz, [b] Sándor Biri, [b] Zuzana Kaňuchová, [d] Robert W. McCullough, [e] Bhalamurugan Sivaraman, [c] Sergio Ioppolo [fg] and Nigel J. Mason *[ab]

Received 6th July 2023,
Accepted 16th September 2023

DOI: 10.1039/d3cp03196a

rsc.li/pccp

The use of mid-infrared spectroscopy to characterise the chemistry of icy interstellar and Solar System environments will be exploited in the near future to better understand the chemical processes and molecular inventories in various astronomical environments. This is, in part, due to observational work made possible by the recently launched *James Webb Space Telescope* as well as forthcoming missions to the outer Solar System that will observe in the mid-infrared spectroscopic region (*e.g.*, the *Jupiter Icy Moons Explorer* and the *Europa Clipper* missions). However, such spectroscopic characterisations are crucially reliant upon the generation of laboratory data for comparative purposes. In this paper, we present an extensive mid-infrared characterisation of SO_2 ice condensed at several cryogenic temperatures between 20 and 100 K and thermally annealed to sublimation in an ultrahigh-vacuum system. Our results are anticipated to be useful in confirming the detection (and possibly thermal history) of SO_2 on various Solar System bodies, such as Ceres and the icy Galilean moons of Jupiter, as well as in interstellar icy grain mantles.

1. Introduction

Spectroscopic techniques are a primary tool in the determination of the chemical compositions of interstellar and Solar System environments, which may in turn provide an insight into the chemical and geophysical processes occurring there. Rotational spectroscopy, for instance, has been effectively used to confirm the presence of at least 270 individual molecular structures within the gas-phase of the interstellar medium.[1,2] In the condensed phase, however, rotational motion is restricted and thus alternative spectroscopic methods must be utilised instead. Mid-infrared transmission absorption spectroscopy has allowed for the identification of about 20 molecules in interstellar icy grain mantles,[3,4] while reflectance absorption spectroscopy has been used extensively in the laboratory study of minerals and molecular ices relevant to Solar System environments.

The recent launch of the *James Webb Space Telescope* offers an unprecedented opportunity to probe the chemical composition of the icy cosmos with extremely sensitive mid-infrared spectroscopic measurements.[4,5] In combination with measurements made by other telescopes working in this spectral range (*e.g.*, the *Spitzer Space Telescope* and the *Infrared Space Observatory*), it is anticipated that much will be revealed with regards to the solid-phase astrochemical processes occurring in dense interstellar clouds, circumstellar discs, icy moons and dwarf planets, comets, and Kuiper Belt objects. Moreover, a number of forthcoming space missions to the outer Solar System will include infrared imaging spectrometers as part of their scientific payloads, and will thus generate copious spectroscopic data. For instance, the *Jupiter Icy Moons Explorer* mission (launched 14th April 2023) contains the MAJIS infrared imaging spectrograph which will be able to observe the surfaces of the Jovian moon system down to a wavenumber of about 1750 cm^{-1}, while the MISE and E-THEMIS instruments aboard the *Europa Clipper* mission to Europa (scheduled launch 10th October 2024) will provide spectroscopic data coverage over the near-, mid-, and far-infrared ranges.

[a] *Centre for Astrophysics and Planetary Science, School of Physics and Astronomy, University of Kent, Canterbury, CT2 7NH, UK. E-mail: mifsud.duncan@atomki.hu, n.j.mason@kent.ac.uk*
[b] *Atomic and Molecular Physics Laboratory, Institute for Nuclear Research (Atomki), Debrecen H-4026, Hungary*
[c] *Atomic, Molecular, and Optical Physics Division, Physical Research Laboratory, Ahmedabad 380009, India*
[d] *Astronomical Institute, Slovak Academy of Sciences, Tatranská Lomnica, SK-059 60, Slovakia*
[e] *Department of Physics and Astronomy, School of Mathematics and Physics, Queen's University Belfast, Belfast, BT7 1NN, UK*
[f] *Centre for Interstellar Catalysis (InterCat), Department of Physics and Astronomy, Aarhus University, Aarhus DK-8000, Denmark*
[g] *School of Electronic Engineering and Computer Science, Queen Mary University of London, London E1 4NS, UK*

However, in order to correctly interpret spectroscopic information gathered by such instruments, it is necessary to have laboratory-generated data with which to compare. To this end, our research group has been active in characterising the mid-infrared spectra of various molecular ices relevant to astrochemistry, including CO_2[6,7] and O_3.[8] In this paper, we build upon our previous work and present a thorough and systematic mid-infrared characterisation of pure SO_2 ice deposited at various cryogenic temperatures and thermally annealed to sublimation. The need for more spectroscopic data on sulphur-bearing astrophysical ice analogues was highlighted in a recent review,[9] and is reflective of our comparatively incomplete understanding of sulphur ice astrochemistry, particularly as it relates to solid SO_2. Indeed, the detection of this molecule in interstellar icy grain mantles is still tentative along many lines of sight due to a lack of multiple matching infrared absorption bands between observational and laboratory data.[3]

When surveying the lines of sight towards the young stellar objects W33A and NGC-7538:IRS1, Boogert and co-workers[10] observed an infrared absorption band whose position and profile were somewhat consistent with that of the ν_3 mode of solid SO_2 either as a pure ice or mixed with CH_3OH. Recently published data from the *James Webb Space Telescope* has also suggested the presence of SO_2 ice in the dense cloud Chamaeleon I along lines of sight towards the background stars NIR38 and J110621, and estimated that the contribution of SO_2 in this cloud to the total sulphur budget was less than 1% of the expected cosmic abundance.[4] The source of interstellar SO_2 ice remains uncertain, but prevailing hypotheses posit it is either the result of direct condensation from the gas phase[10] or the irradiative processing of refractory solids (*e.g.*, elemental sulphur or sulphur-based minerals) that are difficult to observe in the infrared in contact with oxygen-bearing ices.[11,12] Indeed, previous experimental work has suggested that the irradiative processing of SO_2 ice using 1.5 keV electrons results in a relatively facile conversion to infrared-inactive molecular forms of sulphur.[13]

The detection of SO_2 on various Solar System bodies has also proven to be somewhat contentious, due to these observations primarily relying on ultraviolet-visible spectroscopy, which is more ambiguous than infrared spectroscopy in categorically assigning absorption features to particular molecular species. For example, Hendrix *et al.*[14] suggested that the observed ultraviolet-visible reflectance spectra of the dwarf planet Ceres between 320–400 nm could be approximated fairly well by laboratory spectra of phyllosilicate minerals (such as montmorillonite) intermixed with solid SO_2 and allotropic forms of elemental sulphur. Such an interpretation would carry intriguing implications for the Cererian surface and near-subsurface, as it is suggestive of sustained geothermal activity leading to the active outgassing of sulphur-bearing molecules. This interpretation has, however, been met with some resistance. Firstly, none of the infrared bands attributable to SO_2 was detected by the VIR spectrometer aboard the *Dawn* mission.[15] Although such a non-detection is not supportive of the idea of SO_2 ice on the surface of Ceres, it does not necessarily exclude its presence there since these bands could be obscured by dark surface material or could be blended with spectral features assigned to carbonate minerals.[16] However, a further challenge exists in the volatility of SO_2 under Cererian surface conditions: at 201 K, the surface temperature of Ceres is sufficiently high as to drive sublimation and loss of SO_2 without significant re-condensation,[17] and would thus lead to surface patches of SO_2 that are far too small to produce measurable spectral features in global reflectance spectra.[18] In light of its inherent interest to astrobiology, future missions to Ceres equipped with infrared spectrometers have been proposed to better understand the surface composition of the dwarf planet.[19,20]

Solid SO_2 is also present within the outer Solar System, perhaps most famously so on the surfaces of the icy Galilean moons of Jupiter. There, SO_2 chemistry is most extensive on the surface of Io which, as the most volcanically active body in the Solar System, emits about one tonne of sulphur-bearing volcanic ejecta (largely in the form of SO_2 and elemental sulphur) per second.[21] Multiple fates exist for this volcanically-sourced SO_2, including ionisation and dissociation in the Jovian magnetosphere, retention in the Ionian exosphere, or condensation onto the Ionian surface.[22–24] In the case of SO_2 not lost to the Jovian magnetosphere, quotidian temperature variations on Io allow for SO_2 to be cycled between the surface and the exosphere. During the day, when temperatures are warmer, sublimation of surface SO_2 ice populates the exosphere along with trace quantities of SO, S_2, NaCl, and KCl.[25] As temperatures drop during the night or during an eclipse, much of this exosphere then collapses due to the condensation of the SO_2 back to the surface.[25] Thoroughly characterised mid-infrared spectra of SO_2 at different temperatures will thus aid in further comprehending the SO_2 cycle on Io.

Such spectra would also be useful in further elucidating the distribution and chemistry of SO_2 on the surface of the neighbouring Galilean moon Europa, where it is thought to participate in an ongoing radiation-driven process in which sulphur is cycled between various molecular forms (including SO_2, H_2SO_4 hydrates, and elemental sulphur) as a result of the interaction of incident ionising radiation supplied by the giant Jovian magnetosphere with the surface.[26,27] Due to the ability of sulphur to adopt a number of different oxidation states, the oxides of sulphur (including SO_2) are able to participate in a rich redox chemistry.[28] Many of these redox reactions are thermally viable under cryogenic conditions such as those expected on the surfaces of icy outer Solar System bodies[28–35] and may thus be important drivers of chemical disequilibrium in these environments.[36–40] Therefore, confirming the detection of SO_2 on outer Solar System bodies of astrobiological interest is crucial to accurately assessing the potentially life-sustaining redox chemistry that occurs there. To date, however, studies of the presence and distribution of SO_2 across the surface of Europa have exclusively relied on ultraviolet-visible spectroscopy[41–43] which, as previously mentioned, is not ideally suited for the unambiguous identification of molecular species.

There therefore exists a strong motivation to produce laboratory-generated mid-infrared spectroscopic data to support

Table 1 Summary of the major mid-infrared absorption features of SO_2 ice (and some isotopologues). Band peak positions for selected ices investigated in this study (amorphous ice at 20 K and crystalline ice at 100 K) are also included for comparative purposes

		Band position (cm^{-1})									
										This study	
Mode	Assignment	Reference A	Reference B	Reference C	Reference D	Reference E	Reference F	Reference G	Reference H	Amorphous	Crystalline
ν_1	$^{32}S^{18}O^{16}O$	—	—	—	—	1122	1121	1120.6	1121.5	—	1120.5
	$^{34}S^{16}O_2$	—	1140.1	1140.5	1140.0	1141	1140	1140.4	—	—	1140.0
	$^{32}S^{16}O_2$ A_1 (TO)	1145.8	1142.8	1147.0	1143.0	1144	1144	1144.8	—	1147.5	1142.8
	$^{32}S^{16}O_2$ A_1 (LO)	—	—	1160.0	1150.0	1148	—	—	1148.0	—	1149.1
ν_2	$^{32}S^{18}O^{16}O$	—	—	—	—	—	—	514.3	—	—	—
	$^{34}S^{16}O_2$	—	—	517.0	—	—	517	—	—	—	—
	$^{32}S^{16}O_2$ A_1 (TO)	520.1	520.8	525.0	522.7	524	521	522.0	525.4	—	—
	$^{32}S^{16}O_2$ A_1 (LO)	—	—	546.0	530.0	542	528	—	533.1	—	—
ν_3	$^{36}S^{16}O_2$	—	—	—	—	—	—	1288.8	—	—	—
	$^{32}S^{18}O^{16}O$	—	1302.8	—	1302.8	—	—	—	—	—	1302.8
	$^{34}S^{16}O_2$	—	1304.5	1304.0	1304.3	1304	1303	1302.8	1305.8	—	1304.8
	$^{32}S^{16}O_2$ B_1 (TO)	1315.5	1310.8	1313.0	1310.1	1312	1310	1315.2	1316.4	—	1311.9
	$^{32}S^{16}O_2$ B_2 (TO)	—	1321.6	1327.0	1323.3	1324	1322	1323.2	1329.6	1323.7	1323.4
	$^{32}S^{16}O_2$ B_2 (LO)	—	—	1358.0	1345.0	1341	1334	—	—	—	1342.4
$\nu_1 + \nu_2$	$^{32}S^{16}O_2$	1607.6	1611.3	—	—	—	—	—	—	1609.7	1609.7
$\nu_1 + \nu_3$	$^{34}S^{16}O_2$	—	2433.7	—	2433.7	—	2432	2433.5	2435.5	—	2433.8
	$^{32}S^{16}O_2$	2455.8	2456.2	2457.4	2456.2	—	2455	2456.5	2456.7	2456.9	2456.7
$\nu_2 + \nu_3$	$^{32}S^{16}O_2$	—	—	—	—	—	—	—	1850.1	—	—
$2\nu_1 + \nu_3$	$^{32}S^{16}O_2$	—	3584.5	—	—	—	—	—	—	—	—
$2\nu_1$	$^{34}S^{16}O_2$	—	2273.9	—	2273.9	—	—	2274.3	—	—	—
	$^{32}S^{16}O_2$	2288.4	2287.4	2288.2	2287.4	—	2287	2288.0	2289.7	—	2287.4

Reference A: Schriver-Mazzuoli *et al.*[44] for an amorphous ice at 30 K. Reference B: Schriver-Mazzuoli *et al.*[44] for a crystalline ice at 90 K. Reference C: Anderson and Campbell[51] for a crystalline ice at 20 K. Reference D: Khanna *et al.*[52] for a crystalline ice at 90 K. Reference E: Anderson and Savoie[53] for a crystalline ice at 77 K. Reference F: Giguère and Falk[54] for a crystalline ice at 98 K. Reference G: Barbe *et al.*[45] for a crystalline ice at 77 K. Reference H: Nash and Betts[48] for a crystalline ice at 80 K.

the detection of SO_2 in observed interstellar and outer Solar System ices. Indeed, the mid-infrared absorption spectroscopy of pure SO_2 ice was studied by Schriver-Mazzuoli *et al.*,[44] who have arguably provided the most detailed spectroscopic analysis of this ice to date by considering the reflectance absorption spectroscopy of SO_2 deposited at 11 and 30 K and thermally annealed to higher temperatures. They found that, at 30 K, amorphous SO_2 ice presents three fundamental absorption bands associated with the symmetric stretching (ν_1), bending (ν_2), and antisymmetric stretching (ν_3) modes respectively located at 1145.8, 520.1, and 1315.5 cm^{-1}. These values match fairly well (within 5 cm^{-1}) with those reported by older studies (Table 1). Thermal annealing of a low temperature amorphous SO_2 ice results in its crystallisation at temperatures above 70 K, resulting in a narrowing of the stretching mode bands and the development of band sub-structures attributable to various SO_2 isotopologues and the LO-TO splitting† of the $^{32}S^{16}O_2$ bands.[44–46] Other mid-infrared spectroscopic studies have also been performed with the aim of characterising higher frequency overtone and combination bands[47,48] or the structure of the SO_2 dimer.[49,50]

In order to better detect the presence of SO_2 ice in various astronomical environments and assess its thermal history, systematic and quantitative laboratory studies of its mid-infrared spectroscopy under different deposition and thermal annealing conditions are required. Such laboratory-generated data will not only aid in better defining the sulphur content of the cosmos, but will also provide insights into the chemical and geophysical conditions of various planetary-like bodies that are of current astrobiological interest. Such work is the objective of this paper, wherein we present an analysis of mid-infrared spectroscopic data acquired during the thermal annealing of pure SO_2 ices deposited at 20, 40, 70, and 100 K under ultrahigh-vacuum conditions, with a particular focus on the ν_1 and ν_3 fundamental modes and the $\nu_1 + \nu_3$ combination mode.

† Phonons may result from long-range collective vibrations in a solid lattice. Phonons are quantised vibrations in which lattice molecules vibrate at a single frequency. Optical phonons occur when molecules are moving out of phase within the lattice, and may propagate either parallel (longitudinal optical; LO) or perpendicular (transverse optical; TO) to the direction of the incident infrared field. This is manifested as a splitting of a number of infrared absorption bands.

2. Experimental methodology

Experimental work was carried out using the Ice Chamber for Astrophysics–Astrochemistry (ICA); a set-up for laboratory

astrochemistry located at the Institute for Nuclear Research (Atomki) in Debrecen, Hungary. The set-up has been described in detail in previous publications,[29,55] and so only a brief overview of its most salient features is provided in this paper. The ICA is an ultrahigh-vacuum-compatible chamber with a base pressure of a few 10^{-9} mbar which is maintained by the combined action of a turbomolecular pump and a scroll pump. Within the centre of the chamber is a gold-coated oxygen-free high-conductivity copper sample holder into which up to four ZnSe deposition substrates may be mounted. The sample holder is held in contact with the cold finger of a closed-cycle helium cryostat which allows it to be cooled to 20 K. Temperature regulation in the range 20–300 K is achieved by setting an equilibrium between an internal cartridge heater and the cooling effect of the cryostat.

Pure SO_2 ices were prepared on the cooled ZnSe deposition substrates *via* background deposition of SO_2 gas (99.8% purity, Linde). The gas was first introduced into a pre-mixing line before being dosed into the main chamber at a pressure of a few 10^{-6} mbar, which corresponds to an average ice thickness growth rate of approximately 0.03 μm min^{-1}. The growth (and subsequent thermal annealing) of the ices were monitored *in situ* by Fourier-transform mid-infrared transmission absorption spectroscopy (spectral range = 4000–650 cm^{-1}; resolution = 0.5 cm^{-1}) using a Thermo Nicolet Nexus 670 spectrophotometer and by maintaining the infrared spectroscopic beam at normal incidence to the ice samples. Pure SO_2 ices were deposited at temperatures of 20, 40, 70, and 100 K and then thermally annealed at a rate of 2 K min^{-1}, with mid-infrared spectra being acquired at successive 10 K intervals until complete sublimation of the ice was recorded. Prior to acquiring a mid-infrared spectrum at a given temperature, the ice was allowed to equilibrate for up to five minutes, during which time no isothermal changes in the appearance of the spectra were noted. A summative list of the experiments performed in this study is provided in Table 2.

The amount of ice deposited in a given experiment could be assessed quantitatively *via* the mid-infrared spectra collected just after deposition of the ice prior to any thermal annealing. The molecular column density N (molecules cm^{-2}) of a deposited ice is related to the band area P (cm^{-1}) of a characteristic mid-infrared absorption band as follows:

$$N = \frac{P\ln(10)}{A_\nu} \quad (1)$$

where A_ν is the integrated band strength constant (cm $molecule^{-1}$) of the absorption band whose area is being measured. The thickness d (μm) of the deposited ice may then be calculated as:

$$d = 10^4\frac{NM}{\rho N_A} \quad (2)$$

where M is the molar mass of the ice (g mol^{-1}), ρ is the ice density (g cm^{-3}), and N_A is the Avogadro constant (6.02×10^{23} molecules mol^{-1}). In this study, we have taken A_ν to be 7.3×10^{-18} and 4.2×10^{-17} cm $molecule^{-1}$ for the ν_1 and ν_3 modes, respectively; and have taken ρ to be 1.395 and 1.893 g cm^{-1} for amorphous and crystalline SO_2 ice, respectively.[56,57] Uncertainties in the calculated column densities (typically ±12.5%) and ice thickness (on the order of ±0.002 μm) were determined through standard propagation-of-error calculations that assumed a 5% measurement error in the value of P and used published uncertainty values for the values of A_ν and ρ that were used.[56,57]

It should be noted that these values for A_ν were calculated for amorphous SO_2 ices deposited at 10 K,[56] while the ρ values for amorphous and crystalline SO_2 were measured for ices deposited at 19 and 85 K,[56,57] respectively. It is, however, likely that the values of A_ν and ρ vary as a function of temperature. Indeed, such variations have been systematically measured for other ices (*e.g.*, CH_3OH and CO) over defined temperature ranges.[58,59] To the best of our knowledge, however, no previous study has undertaken the systematic measurement of the A_ν and ρ values of SO_2 ice at different temperatures. In the absence of such a study, the magnitude of the uncertainty introduced into our column density and ice thickness measurements as a result of using A_ν and ρ values defined for SO_2 ices deposited at temperatures that differ from those being studied is unclear; although it is important to note that this should not affect the spectroscopic characterisations of the major SO_2 absorption bands discussed in this paper.

Table 2 Summary of the thermally annealed SO_2 ices considered in this study. Uncertainties in the thicknesses of the ices are estimated to be on the order of ±0.002 μm

SO_2 Ice	Deposition T (K)	N (10^{17} molecules cm^{-2})	d (μm)
1	20	6.25 ± 0.78	0.48
2	40	5.71 ± 0.72	0.44
3	70	6.34 ± 0.80	0.36
4	100	5.58 ± 0.70	0.31

3. Spectroscopic results and discussion

Spectra of amorphous and crystalline SO_2 ices (exemplified by ices respectively deposited at 20 and 100 K) are shown in Fig. 1, which clearly shows the ν_1 and ν_3 fundamental modes and the $\nu_1 + \nu_3$ combination mode. The ν_2 mode, being located at about 520 cm^{-1} (Table 1), is beyond the spectroscopic range of our instrumentation and thus is not considered any further in this study. Interestingly, although very weak absorption features attributable to the $\nu_1 + \nu_2$ combination mode were detected in the spectra of both the amorphous and crystalline ices, the $2\nu_1$ overtone was only visible in the spectrum of the crystalline ice (Fig. 1). Given that the most intense absorption features are likely the most useful for astronomical detections of SO_2, the remainder of this section will be devoted to a detailed mid-infrared spectroscopic characterisation of the ν_1 and ν_3 fundamental modes and the $\nu_1 + \nu_3$ combination mode.

3.1. The antisymmetric stretching (ν_3) mode

The evolution of the SO_2 ν_3 mode as a result of the thermal annealing of ices deposited at 20, 40, 70, and 100 K is shown in

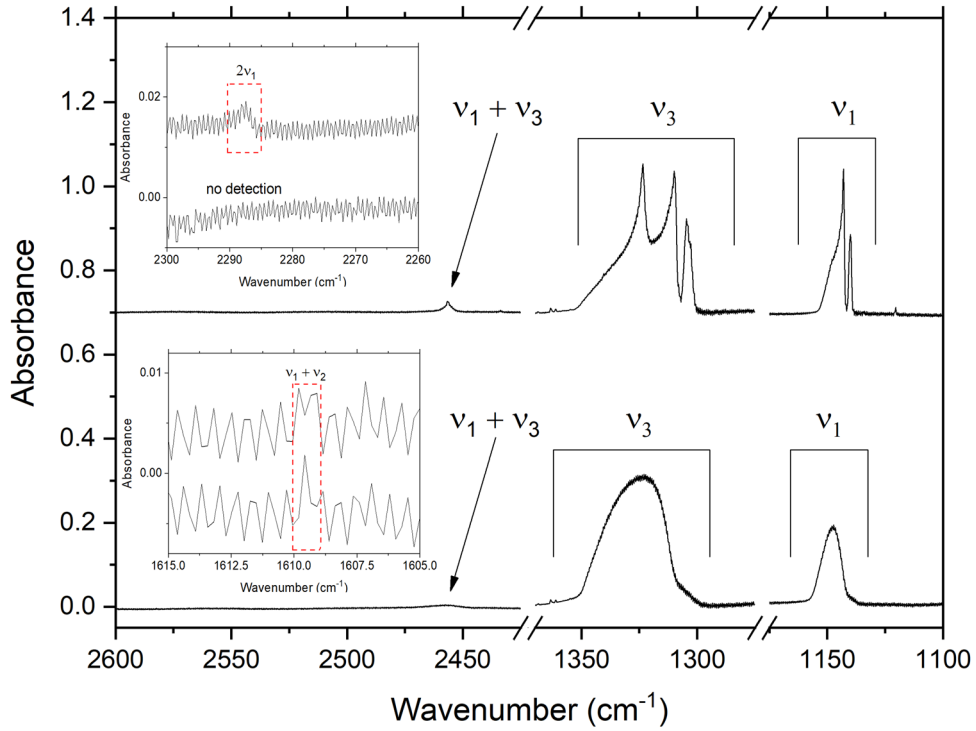

Fig. 1 Mid-infrared spectra of amorphous (lower plot) and crystalline (upper plot) SO_2 ices deposited at temperatures of 20 and 100 K, respectively. Note that the spectra are vertically offset for clarity. The estimated thicknesses of the amorphous and crystalline ices were 0.48 and 0.31 μm, respectively. The insets depict the very weak $2\nu_1$ overtone and $\nu_1 + \nu_2$ combination bands in the amorphous (lower spectra in insets) and crystalline (upper spectra in insets) ices.

Fig. 2. Upon first inspection, it is possible to note that the ices deposited at 20 and 40 K exhibit ν_3 modes that are broad and quasi-symmetric in structure, while those deposited at 70 and 100 K exhibit a number of prominent band sub-structures. Such an observation is indicative of the greater structural order (*i.e.*, crystallinity) of the SO_2 ices deposited at the higher temperatures.

As the ice deposited at 20 K was thermally annealed, a number of changes were noted in the profile, peak position, band area, and peak height of its ν_3 mode. The apparent profile does not vary much upon annealing to 60 K; however, upon further warming to 70 K, the band begins to exhibit some signs of structural ordering in the form of a distinct sub-structure at 1304.8 cm^{-1} attributable to the $^{34}S^{16}O_2$ isotopologue (Table 1). At 80 K, the absorbance of this sub-structure increases and other, higher frequency sub-structures also begin to emerge from the broad band as a result of the more extensive crystallisation of the ice. In particular, two intense features at 1311.9 and 1323.4 cm^{-1} become visible, respectively attributed to the $^{32}S^{16}O_2$ B_1 (TO) and the $^{32}S^{16}O_2$ B_2 (TO) modes.

The changes in the band profile and the emergence of these sub-structures have a marked effect on the total band area and peak height (defined as the height of the most intense sub-structure) of the ν_3 mode (Fig. 3). As the ice was annealed from 20 K, the band peak height H (dimensionless) remained fairly constant up to a temperature of 50 K; within 1% of the original peak height at 20 K. However, upon further thermal annealing, the peak height began to increase until it peaked at 16% greater than its original height at a temperature of 100 K. Beyond this temperature, the peak height decreased due to sublimation losses of the ice and, indeed, the ice had fully sublimed by a temperature of 120 K. The band area P (cm^{-1}), which was measured by integrating over the 1360–1285 cm^{-1} wavenumber range using a linear baseline, exhibited a somewhat different trend: as the ice was annealed from 20 to 50 K, the band area decreased by about 8% of its original value. It then increased to approximately its original value as it was heated to 70 K, dipped slightly at 80 K, and then peaked at 6% greater than its original value at a temperature of 90 K. At higher temperatures, the band area decreased likely due to losses to sublimation of the ice.

Analysis of the band peak position was also carried out by considering the wavenumber position of the peak of the broad band in the case of amorphous SO_2 ices, and the peak of the emergent $^{32}S^{16}O_2$ B_2 (TO) mode in the case of the ices exhibiting some degree of structural order (Fig. 3). When annealed from 20 K, the ν_3 band does not significantly vary in its wavenumber position until a temperature of 40 K is exceeded, after which the band red-shifts by approximately 2 cm^{-1}. Interestingly, this red-shift was only observed at temperatures greater than 40 K but below 70 K, and the band returned to within 0.5 cm^{-1} of its original position upon deposition at 20 K at higher temperatures. Our analysis would therefore seem to suggest that, when deposited at 20 K and thermally annealed to

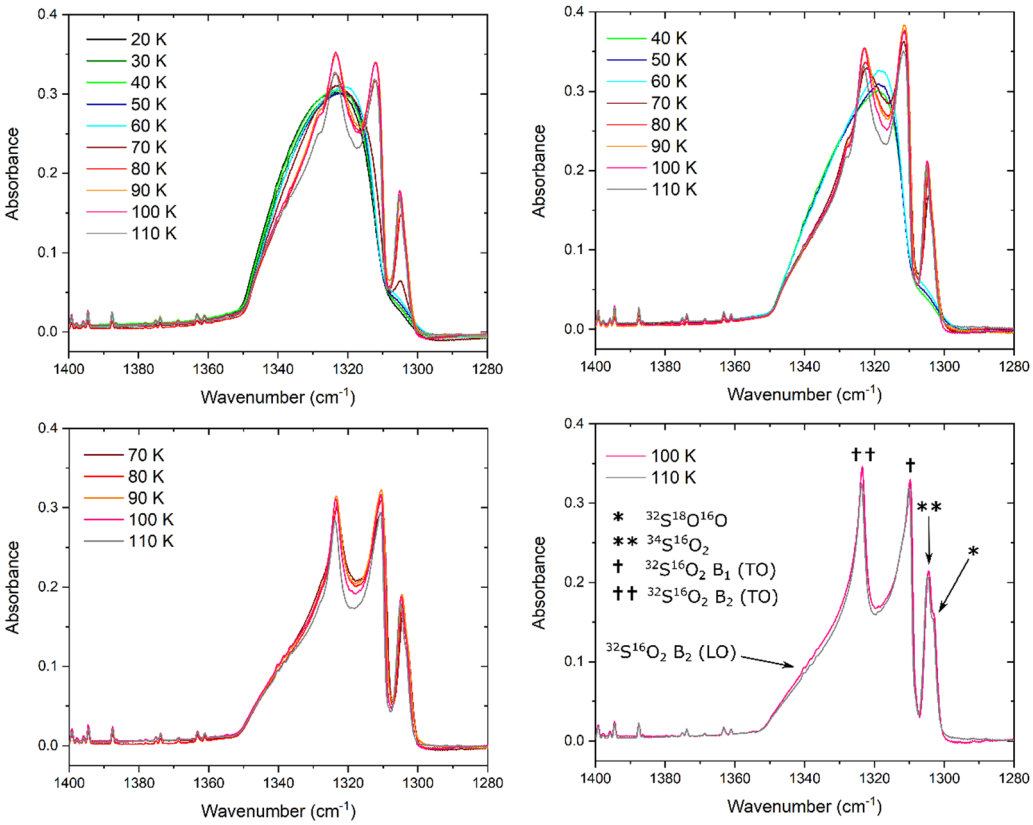

Fig. 2 Thermal evolution of the SO_2 ν_3 band for ices deposited at 20, 40, 70, and 100 K.

higher temperatures, SO_2 ice remains an amorphous solid up to a temperature of 40 K after which the ice undergoes a structural reorganisation to a crystalline phase which appears to be complete by 70 K.

The ν_3 band of the SO_2 ice deposited at 40 K exhibits similar trends during its thermal annealing (Fig. 2 and 3), although a number of subtle differences are evident. For instance, the peak height of the band was noted to increase significantly more rapidly during thermal annealing to 70 K compared to the analogous thermal annealing of the ice deposited at 20 K. We speculate that this is due to a change in the apparent band strength which manifests as a greater peak height. Under our experimental conditions, a change in the apparent band strength over this temperature range is believed to be reflective of the reduction of the number of pores in the ice structure leading to absorption more akin to that of a perfect crystalline solid. This decrease in ice porosity is referred to as compaction and may be induced in astrophysical ice analogues as a result of their thermal annealing[60,61] or irradiation.[62] In our experiments, it is possible that the rate of pore collapse and ice compaction as a result of thermal annealing in the SO_2 ice deposited at 40 K was more rapid than that in the ice deposited at 20 K, thus leading to a more rapid increase in the peak height of the ν_3 mode. Indeed, a similar observation was noted when analysing the ν_1 band of the SO_2 ices deposited at 20 and 40 K (Fig. 4), which is consistent with this interpretation. We emphasise that this explanation is speculative, and that additional tests on the porosity of the deposited SO_2 ices are required to confirm or refute it.

Another difference between the spectroscopic data collected for the ν_3 band of the ices deposited at 20 and 40 K lies in the profile of the band at 70 K. For the former ice, this band is still largely broad and featureless with a small sub-structure due to the $^{34}S^{16}O_2$ isotopologue being recorded at approximately 1305 cm^{-1} (Fig. 2). However, upon thermal annealing of the SO_2 ice deposited at 40 K to 70 K, the ν_3 band presents a structured profile with new and intense sub-structures attributable to the $^{32}S^{16}O_2$ B_1 (TO) and the $^{32}S^{16}O_2$ B_2 (TO) modes, as well as the $^{34}S^{16}O_2$ isotopologue, being observed. Hence, the thermal annealing of a SO_2 ice to 70 K results in more extensive crystallisation if the ice was initially deposited at 40 K compared to 20 K. Beyond 70 K, the trends observed with regards to band area and peak height of the SO_2 ice deposited at 40 K are similar to those observed for the ice deposited at 20 K.

It is interesting to note that, upon thermal annealing of the ice deposited at 40 K to 70 K, the band peak position of the SO_2 ν_3 mode blue-shifts from 1319.4 to 1322.2 cm^{-1}. The band peak continues to blue-shift upon further thermal annealing, with a blue-shift of 3.8 cm^{-1} relative to its position upon deposition being observed at 110 K (Fig. 3). This change in the position of the ν_3 band peak is significantly greater than those observed during the thermal annealing of SO_2 ices deposited at any other temperature which, with the exception of a red-shift of less than 2 cm^{-1} between 40 and 70 K for the ice deposited at 20 K,

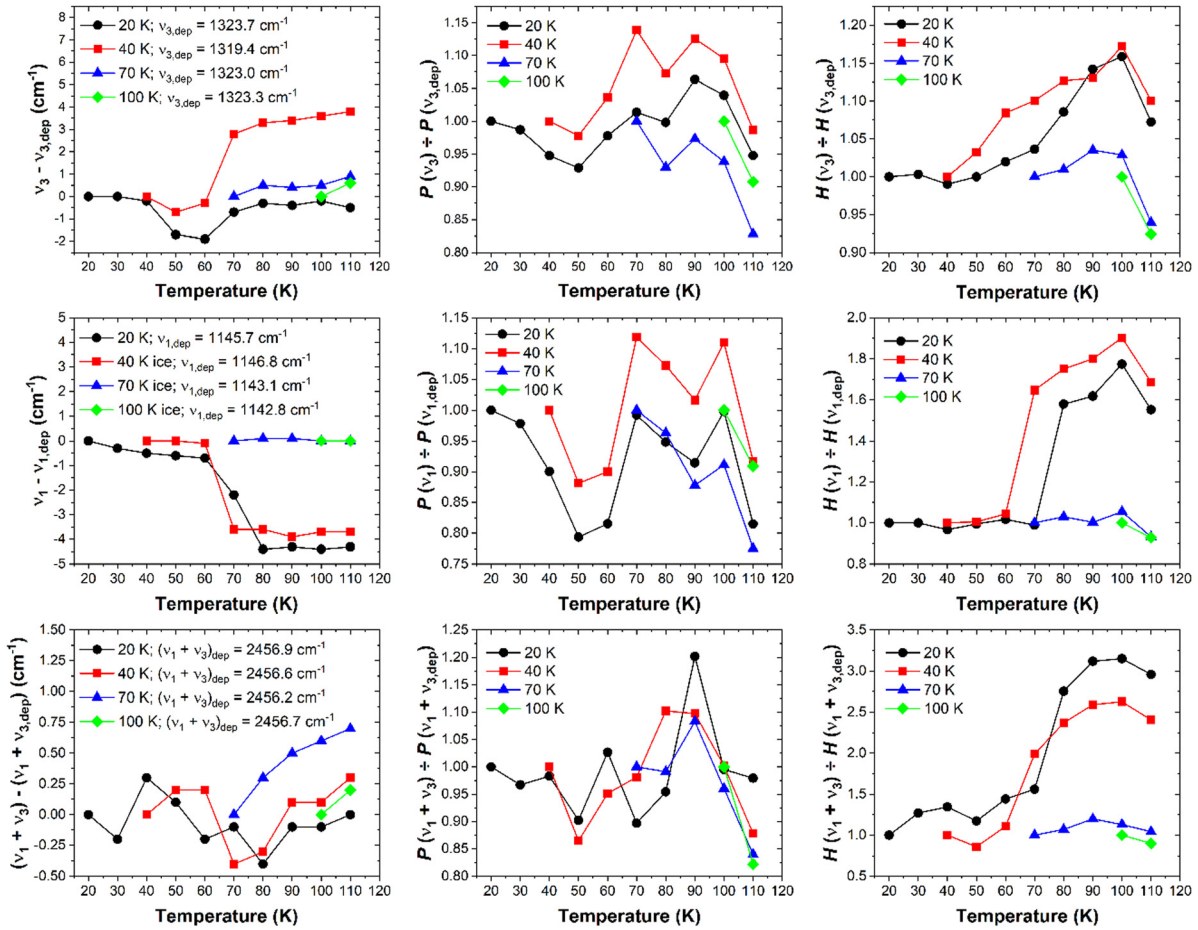

Fig. 3 Variations in the position (left panels), band area (centre panels), and peak height (right panels) of the ν_3 (top panels), ν_1 (middle panels), and $\nu_1 + \nu_3$ (bottom panels) bands of SO_2 ices deposited at 20 (black circles), 40 (red squares), 70 (blue triangles), and 100 K (green diamonds) relative to the value of these parameters at the deposition temperature of each of these ices. Error bars have been omitted for clarity, but upper bounds to the uncertainties associated with the terms $\nu_n - \nu_{n,dep}$ and $P(\nu_n)/P(\nu_{n,dep})$ have been calculated to be ± 0.14 cm^{-1} and $\pm 7\%$, respectively. For the $H(\nu_n)/H(\nu_{n,dep})$ term, an uncertainty of $\pm 1\%$ has been calculated for the fundamental modes, while a larger uncertainty of $\pm 7\%$ has been calculated for the combination mode.

typically remained within 1 cm^{-1} of their position upon deposition (Fig. 3). A reason for the observed blue-shift in the data for the ice deposited at 40 K is difficult to provide with any certainty, although it is possibly related to structural changes occurring within the ice over a short temperature range.

Lastly, the ν_3 modes of the ices deposited at 70 and 100 K present profiles containing well-defined sub-structures indicative of extensive structural ordering (Fig. 2). Indeed, the band areas and peak heights for these ices follow thermal annealing trends that are qualitatively similar to those observed in the ices deposited at lower temperatures, although they vary to a significantly lesser degree relative to their original values at deposition (Fig. 3). Moreover, the peak positions did not drastically shift, and remained within 1 cm^{-1} of their original position upon deposition. The ν_3 modes of the ices deposited at 70 and 100 K do, however, exhibit a more evident band at about 1303 cm^{-1} attributed to the $^{32}S^{18}O^{16}O$ isotopologue, as well as a shoulder at about 1342 cm^{-1} due to the $^{32}S^{16}O_2$ B_2 (LO) mode.

3.2. The symmetric stretching (ν_1) mode

The evolution of the SO_2 ν_1 mode during the thermal annealing of SO_2 ices deposited at 20, 40, 70, and 100 K is shown in Fig. 4. The variations in the profile of this band mirror and complement those observed with regards to the ν_3 mode. For example, no significant changes in the band profile, position (measured by considering the wavenumber position of the peak of the broad band in the case of amorphous SO_2, and the peak of the emergent $^{32}S^{16}O_2$ A_1 (TO) mode in the case of the ices exhibiting greater degrees of structural order), or peak height (Fig. 3 and 4) were noted upon thermal annealing of the ice deposited at 20 K to 60 K; however, the band area (measured by integrating over the 1165–1120 cm^{-1} wavenumber range using a linear baseline) did decrease by approximately 20% of its original value over this temperature range. Once the ice was warmed to 70 K, the emergence of new sub-structures attributable to the $^{32}S^{18}O^{16}O$ and $^{34}S^{16}O_2$ isotopologues was observed.

A red-shift of about 2 cm^{-1} in the peak position of the ν_1 band was observed upon warming the ice to 70 K, and a

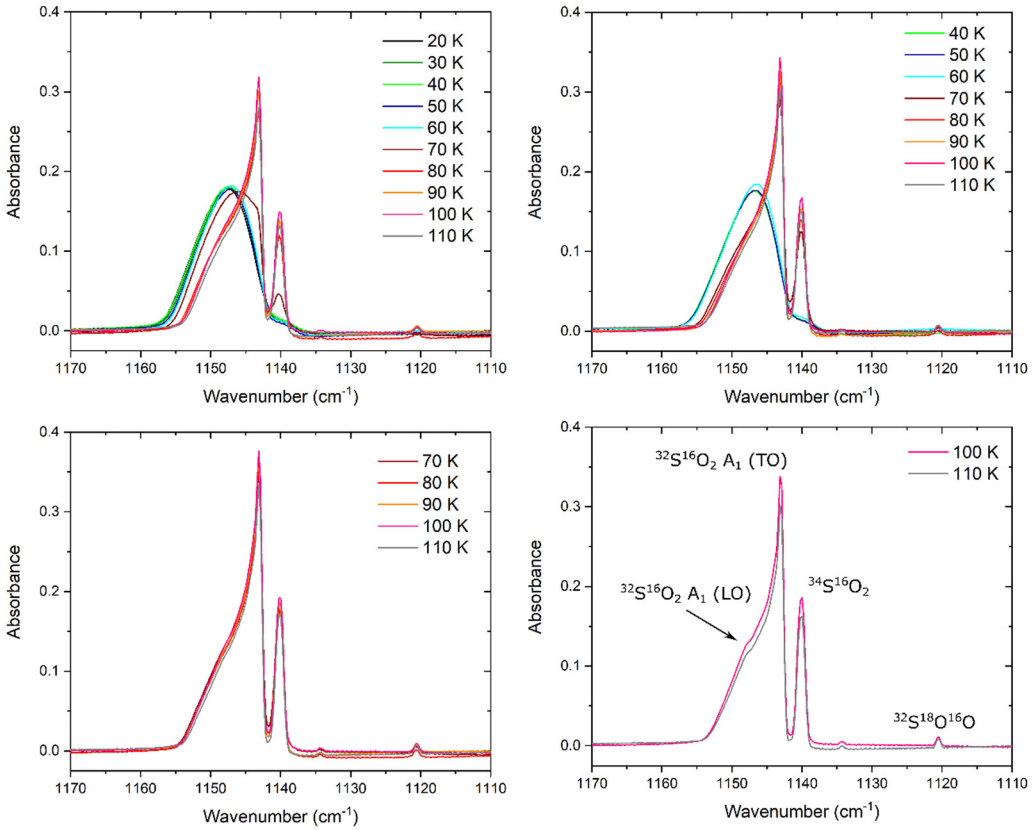

Fig. 4 Thermal evolution of the SO_2 ν_1 band for ices deposited at 20, 40, 70, and 100 K.

red-shift of an additional 2 cm^{-1} was observed upon further annealing to 80 K (Fig. 3). At 80 K, the ν_1 band contains several distinct sub-structures and has a peak height which is approximately 60% greater than its original value at 20 K, although the band area has more or less recovered to its original value. Aside from the sub-structures attributed to the $^{32}S^{18}O^{16}O$ and $^{34}S^{16}O_2$ isotopologues and the $^{32}S^{16}O_2$ A_1 (TO) mode, a shoulder is present at about 1149 cm^{-1} due to the emergence of the $^{32}S^{16}O_2$ A_1 (LO) mode (Fig. 4).

Similarly to the SO_2 ice deposited at 20 K, the ν_1 band of the ice deposited at 40 K exhibits negligible changes in its apparent profile, position, or peak height upon thermal annealing to 60 K. However, upon further warming to 70 K, the peak height of the band increases by about 60% of its original value and the band red-shifts by approximately 3.5 cm^{-1} to lower wavenumbers. At 70 K, a distinction between the profiles of the SO_2 ν_1 band of the ices deposited at 20 and 40 K exists in the more pronounced appearance of the band attributed to the $^{34}S^{16}O_2$ isotopologue in the case of the latter, which is indicative of a more structurally ordered (*i.e.*, crystalline) ice. This observation mirrors that made with regards to the ν_3 mode of the $^{34}S^{16}O_2$ isotopologue (Fig. 2), and is further evidence of the fact that thermally induced crystallisation in an ice is more efficient if the initially amorphous ice was deposited at higher temperatures.

The evolution of the band area of the ν_1 mode of the SO_2 ice deposited at 40 K as a result of its thermal annealing is qualitatively similar to that of the SO_2 ice deposited at 20 K, with a slightly decreased area (relative to its value upon deposition) over the 40–60 K temperature range followed by a large increase when heated to 70 K. This increase in band area is most probably associated with the thermally induced crystallisation process taking place which is largely complete by 70 K. The most significant decreases in the area of the ν_1 band occurred at temperatures greater than 100 K due to some sublimation of the ice, with full ice desorption recorded by 120 K. These observations are consistent with those made with regards to the ν_3 mode.

Lastly, it is to be noted that the ν_1 bands of the SO_2 ices deposited at 70 and 100 K appeared to indicate that the ice was in a crystalline phase throughout the thermal annealing process, with negligible changes in the band profile, position, and peak height being observed (Fig. 3 and 4). This is confirmed by the fact that sub-structures attributable to the $^{32}S^{16}O_2$ A_1 (TO) and the $^{32}S^{16}O_2$ A_1 (LO) modes, as well as the $^{34}S^{16}O_2$ and the $^{32}S^{18}O^{16}O$ isotopologues, were clearly identifiable in both these ices throughout thermal annealing until the ices sublimed (Fig. 4).

3.3. The $\nu_1 + \nu_3$ combination mode

We have also analysed the weak $\nu_1 + \nu_3$ combination mode band and its response to thermal annealing for ices deposited at 20, 40, 70, and 100 K (Fig. 5). This analysis complements our findings with regards to the ν_1 and ν_3 fundamental bands.

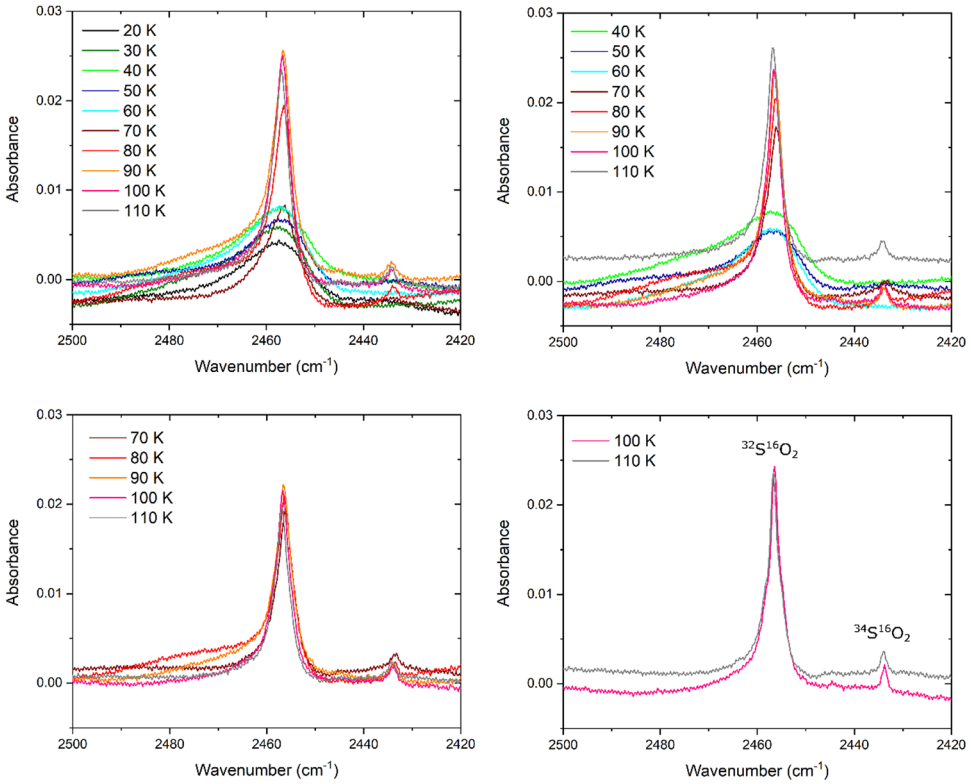

Fig. 5 Thermal evolution of the SO_2 $\nu_1 + \nu_3$ band for ices deposited at 20, 40, 70, and 100 K.

At 20 K, the combination band adopts a broad structure which is retained upon thermal annealing of the ice to 60 K. Beyond this temperature, the band assumes a narrower profile whose peak height more than triples compared to its original value at 20 K, although the band position does not change by a significant amount. A satellite band at about 2434 cm^{-1} becomes evident at 80 K, and is ascribed to the $^{34}S^{16}O_2$ isotopologue (Fig. 5).

The position of the $\nu_1 + \nu_3$ band does not shift by more than 1 cm^{-1} during the thermal processing of each of the investigated ices, irrespective of the deposition temperature (Fig. 3). It is also evident that the band area (measured by integrating over the 2500–2420 cm^{-1} wavenumber range using a linear baseline) does not change by more than 20% of its original value during thermal annealing of the studied ices (Fig. 3). Although a 20% change in the band area may seem significant, it must be recalled that this combination band is a fairly weak absorption feature and thus a 20% change in the band area does not necessarily correspond to any significant change in the profile of the band in absolute terms.

The descriptive parameter of the $\nu_1 + \nu_3$ combination band which provides the most information on the structural changes occurring within the ice during thermal annealing is therefore the band peak height (Fig. 3). For amorphous SO_2 ices prepared by deposition at 20 and 40 K, the greatest increases in peak height occur over the 60–80 K range, whereas the peak height remains fairly constant in the cases of the ices deposited at 70 and 100 K. Furthermore, it is also possible to notice differences in the evolution of the satellite band at about 2434 cm^{-1} as a result of the thermal annealing of the ices based on the temperature at which the ice was deposited. In the case of the ice deposited at 20 K this band was not visible until a temperature of 80 K had been reached, while in the case of the ice deposited at 40 K this band was first observed at 70 K but only fully emerged against the background at 80 K. This is further evidence of greater structural order induced in an amorphous SO_2 ice as a result of its thermal annealing if it was initially deposited at 40 K rather than 20 K (*i.e.*, if it was initially deposited at a higher temperature compared to a lower one). The $^{34}S^{16}O_2$ $\nu_1 + \nu_3$ combination band was present and identifiable in the spectra of the ices deposited at 70 and 100 K throughout the thermal annealing experiments, thus indicating that these ices were crystalline in nature.

4. Conclusions

In this study, we have performed a thorough and systematic mid-infrared spectroscopic analysis of the ν_1 and ν_3 fundamental absorption modes and the $\nu_1 + \nu_3$ combination mode of SO_2 ices deposited at temperatures and thermally annealed under conditions relevant to astrochemistry. Our results have demonstrated that the ices deposited at lower temperatures (*i.e.*, 20 and 40 K), which are initially amorphous, undergo a thermally induced structural reorganisation to a crystalline phase over a temperature range of 40–70 K. The degree of crystallinity

induced in thermally annealed amorphous ices is dependent upon the initial temperature of preparation, with amorphous ices deposited at higher temperatures undergoing more extensive crystallisation as a result of thermal annealing. This was particularly apparent in the case of the ν_1 and ν_3 modes of the $^{34}S^{16}O_2$ isotopologue which, at 70 K, were clearly defined in the case of the SO_2 ice initially deposited at 40 K but were much broader and of lower intensity in the case of the ice initially deposited at 20 K. SO_2 ices initially deposited at 70 and 100 K appeared to be crystalline throughout the entire thermal annealing process.

Our work is of direct relevance to the detection of SO_2 ice in the cosmos and the elucidation of the thermal history of such ices. For instance, our spectroscopic observations may prove useful when analysing data collected by the recently launched *James Webb Space Telescope* and may thus allow for secure identifications of SO_2 ice in dense interstellar clouds. Moreover, forthcoming missions within the Solar System, such as the *Jupiter Icy Moons Explorer* and *Europa Clipper* missions to the Jovian system, will be equipped with infrared imaging spectrometers which may allow for the detection of solid SO_2 on the surfaces of icy moons that are presently considered to be potential abodes of extra-terrestrial life, such as Europa and Ganymede. Finally, we intend to follow up on this work by performing systematic mid-infrared spectroscopic studies of other simple inorganic sulphur-bearing molecules that are relevant to astrochemistry, such as H_2S.

Author contributions

The experimental project was designed by Duncan V. Mifsud and was carried out by Duncan V. Mifsud, Péter Herczku, K. K. Rahul, and Sándor T. S. Kovács, with additional support received from Ragav Ramachandran, Pavithraa Sundararajan, Richárd Rácz, and Sándor Biri. Data analysis was performed by Duncan V. Mifsud and Zuzana Kaňuchová. Béla Sulik, Zoltán Juhász, and Nigel J. Mason supervised the project. The manuscript was prepared by Duncan V. Mifsud. All authors took part in discussions relating to the interpretation of the results, their applicability to observational astrochemistry, and the improvement of the manuscript.

Conflicts of interest

There are no conflicts to declare.

Acknowledgements

The authors gratefully acknowledge funding from the Europlanet 2024 RI which has been funded by the European Horizon 2020 Research Innovation Programme under grant agreement No. 871149. The main components of the experimental apparatus were purchased using funding obtained from the Royal Society through grants UF130409, RGF/EA/180306, and URF/R/191018. Recent developments of the set-up were supported in part by the Eötvös Loránd Research Network through grants ELKH IF-2/2019 and ELKH IF-5/2020. We also acknowledge support from the National Research, Development, and Innovation Fund of Hungary through grant agreement No. K128621. This paper is also based on work from the COST Action CA20129 MultIChem, supported by COST (European Cooperation in Science and Technology). Duncan V. Mifsud is the grateful recipient of a University of Kent Vice-Chancellor's Research Scholarship. Ragav Ramachandran and Pavithraa Sundararajan would like to acknowledge the support of Anil Bhardwaj through his J.C. Bose Fellowship that allowed them to work at PRL as visiting scientists. Zoltán Juhász is grateful for the support of the Hungarian Academy of Sciences through the János Bolyai Research Scholarship. The research of Zuzana Kaňuchová is supported by the Slovak Grant Agency for Science (grant agreement No. 2/0059/22) and the Slovak Research and Development Agency (contract No. APVV-19-0072). Bhalamurugan Sivaraman is thankful for the support received from INSPIRE (grant agreement No. IFA-11 CH-11). Sergio Ioppolo thanks the Danish National Research Foundation through the Centre of Excellence 'InterCat' (grant agreement No. DNRF150) and the Royal Society for financial support.

References

1 B. A. McGuire, *Astrophys. J., Suppl. Ser.*, 2022, **259**, 30.
2 R. C. Fortenberry, *Int. J. Quantum Chem.*, 2017, **117**, 81.
3 A. C. A. Boogert, P. A. Gerakines and D. C. B. Whittet, *Annu. Rev. Astron. Astrophys.*, 2015, **53**, 541.
4 M. K. McClure, W. R. M. Rocha, K. M. Pontoppidan, N. Crouzet, L. E. U. Chu and E. Dartois, *et al.*, *Nat. Astron.*, 2023, **7**, 431.
5 Y. L. Yang, J. D. Green, K. M. Pontoppidan, J. B. Bergner, L. I. Cleeves and N. J. Evans, *et al.*, *Astrophys. J., Lett.*, 2022, **941**, L13.
6 S. Ioppolo, J. A. Noble, A. Traspas Muiña, H. M. Cuppen, S. Coussan and B. Redlich, *J. Mol. Spectrosc.*, 2022, **385**, 111601.
7 D. V. Mifsud, Z. Kaňuchová, S. Ioppolo, P. Herczku, A. Traspas Muiña and T. A. Field, *et al.*, *J. Mol. Spectrosc.*, 2022, **385**, 111599.
8 D. V. Mifsud, Z. Kaňuchová, S. Ioppolo, P. Herczku, A. Traspas Muiña, B. Sulik, K. K. Rahul, S. T. S. Kovács, P. A. Hailey, R. W. McCullough, N. J. Mason and Z. Juhász, *Phys. Chem. Chem. Phys.*, 2022, **24**, 18169.
9 D. V. Mifsud, Z. Kaňuchová, P. Herczku, S. Ioppolo, Z. Juhász, S. T. S. Kovács, N. J. Mason, R. W. McCullough and B. Sulik, *Space Sci. Rev.*, 2021, **217**, 14.
10 J. C. Laas and P. Caselli, *Astron. Astrophys.*, 2019, **624**, A108.
11 M. Köhler, A. Jones and N. Ysard, *Astron. Astrophys.*, 2014, **565**, L9.
12 M. Kama, O. Shorttle, A. S. Jermyn, C. P. Folsom, K. Furuya, E. A. Bergin, C. Walsh and L. Keller, *Astrophys. J.*, 2019, **885**, 114.

13 D. V. Mifsud, P. Herczku, R. Rácz, K. K. Rahul, S. T. S. Kovács, Z. Juhász, B. Sulik, S. Biri, R. W. McCullough, Z. Kaňuchová, S. Ioppolo, P. A. Hailey and N. J. Mason, *Front. Chem.*, 2022, **10**, 1003163.
14 A. R. Hendrix, F. Vilas and J. Y. Li, *Geophys. Res. Lett.*, 2016, **43**, 8920.
15 K. Stephan, R. Jaumann, K. Krohn, N. Schmedemann, F. Zambon, F. Tosi, F. G. Carrozzo, L. A. McFadden, K. Otto, M. C. De Sanctis, E. Ammannito, K. D. Matz, T. Roatsch, F. Preusker, C. A. Raymond and C. T. Russell, *Geophys. Res. Lett.*, 2018, **44**, 1660.
16 M. C. De Sanctis, A. Raponi, E. Ammannito, M. Ciarniello, M. J. Toplis and H. Y. McSween, *et al.*, *Nature*, 2016, **536**, 54.
17 J. A. Zhang and D. A. Paige, *Geophys. Res. Lett.*, 2009, **36**, L16203.
18 L. Roth, *Icarus*, 2018, **305**, 149.
19 J. Castillo-Rogez, J. Brophy, K. Miller, M. Sori, J. Scully and L. Quick, *et al.*, *Planet. Sci. J.*, 2022, **3**, 41.
20 O. Gassot, P. Panicucci, G. Acciarini, H. Bates, M. Caballero and P. Cambianica, *et al.*, *Acta Astronaut.*, 2021, **181**, 112.
21 N. Thomas, F. Bagenal, T. W. Hill and J. K. Wilson, in The Io Neutral Clouds and Plasma Torus, *Jupiter: The Planet, Satellites and Magnetosphere*, ed. F. Bagenal, T. Dowling, and W. McKinnon, Cambridge University Press, Cambridge, United Kingdom, 2004.
22 J. F. Cooper, R. E. Johnson, B. H. Mauk, H. B. Garrett and N. Gehrels, *Icarus*, 2001, **149**, 133.
23 C. T. Russell and M. G. Kivelson, *J. Geophys. Res. Planet.*, 2001, **106**, 33267.
24 S. Douté, B. Schmitt, R. Lopes-Gautier, R. Carlson, L. Soderblom, J. Shirley and the Galileo NIMS Team, *Icarus*, 2001, **149**, 107.
25 F. Bagenal and V. Dols, *J. Geophys. Res. Space Phys.*, 2020, **125**, e2019ja027485.
26 R. W. Carlson, R. E. Johnson and M. S. Anderson, *Science*, 1999, **286**, 97.
27 R. W. Carlson, M. S. Anderson, R. E. Johnson, M. B. Schulman and A. H. Yavrouian, *Icarus*, 2002, **157**, 456.
28 S. Oae, *Organic Chemistry of Sulphur*, Plenum Press, New York City (United States), 1977.
29 D. V. Mifsud, Z. Juhász, P. Herczku, S. T. S. Kovács, S. Ioppolo, Z. Kaňuchová, M. Czentye, P. A. Hailey, A. Traspas Muiña, N. J. Mason, R. W. McCullough, B. Paripás and B. Sulik, *Eur. Phys. J. D*, 2021, **75**, 182.
30 M. J. Loeffler and R. L. Hudson, *Geophys. Res. Lett.*, 2010, **37**, L19201.
31 M. J. Loeffler and R. L. Hudson, *Icarus*, 2013, **224**, 257.
32 M. J. Loeffler and R. L. Hudson, *Astrobiology*, 2015, **15**, 453.
33 M. J. Loeffler and R. L. Hudson, *Astrophys. J., Lett.*, 2016, **833**, L9.
34 Z. Kaňuchová, P. Boduch, A. Domaracka, M. E. Palumbo, H. Rothard and G. Strazzulla, *Astron. Astrophys.*, 2017, **604**, A68.
35 J. H. Bang, M. A. Shoaib, C. H. Choi and H. Kang, *ACS Earth Space Chem.*, 2017, **1**, 503.
36 P. D. Tribbett and M. J. Loeffler, *Planet. Sci. J.*, 2022, **3**, 233.
37 L. Schriver-Mazzuoli, A. Schriver and H. Chaabouni, *Can. J. Phys.*, 2003, **81**, 301.
38 M. H. Moore, R. L. Hudson and R. W. Carlson, *Icarus*, 2007, **189**, 409.
39 P. Boduch, R. Brunetto, J. J. Ding, A. Domaracka, Z. Kaňuchová, M. E. Palumbo, H. Rothard and G. Strazzulla, *Icarus*, 2016, **277**, 424.
40 R. Hodyss, P. V. Johnson, S. M. Meckler and E. C. Fayolle, *ACS Earth Space Chem.*, 2019, **3**, 663.
41 A. L. Lane, R. M. Nelson and D. L. Matson, *Nature*, 1981, **292**, 38.
42 A. R. Hendrix, T. A. Cassidy, R. E. Johnson, C. Paranicas and R. W. Carlson, *Icarus*, 2011, **212**, 736.
43 T. M. Becker, S. K. Trumbo, P. M. Molyneux, K. D. Retherford, A. R. Hendrix, L. Roth, U. Raut, J. Alday and M. A. McGrath, *Planet. Sci. J.*, 2022, **3**, 129.
44 L. Schriver-Mazzuoli, H. Chaabouni and A. Schriver, *J. Mol. Struct.*, 2003, **644**, 151.
45 A. Barbe, A. Delahaigue and P. Jouve, *Spectrochim. Acta, Part A*, 1971, **27**, 1439.
46 M. H. Brooker and J. Chen, *Spectrochim. Acta, Part A*, 1991, **47**, 315.
47 B. Schmitt, C. de Bergh and M. Fesjou, *Solar System Ices*, Astrophysics and Space Sciences Library, Kluwer, Dordrecht (The Netherlands), 1998, vol. 227.
48 D. B. Nash and B. H. Betts, *Icarus*, 1995, **117**, 402.
49 M. Wierzejewska-Hnat, A. Schriver and L. Schriver-Mazzuoli, *Chem. Phys.*, 1994, **183**, 117.
50 L. Schriver-Mazzuoli, A. Schriver and M. Wierzejewska-Hnat, *Chem. Phys.*, 1995, **199**, 227.
51 A. Anderson and M. C. W. Campbell, *J. Chem. Phys.*, 1977, **67**, 4300.
52 R. K. Khanna, G. Zhao, M. J. Ospina and J. C. Pearl, *Spectrochim. Acta, Part A*, 1988, **44**, 581.
53 A. Anderson and R. Savoie, *Can. J. Chem.*, 1965, **43**, 2271.
54 P. A. Giguère and M. Falk, *Can. J. Chem.*, 1956, **34**, 1833.
55 P. Herczku, D. V. Mifsud, S. Ioppolo, Z. Juhász, Z. Kaňuchová, S. T. S. Kovács, A. Traspas Muiña, P. A. Hailey, I. Rajta, I. Vajda, N. J. Mason, R. W. McCullough, B. Paripás and B. Sulik, *Rev. Sci. Instrum.*, 2021, **92**, 084501.
56 Y. Yarnall and R. L. Hudson, *Astrophys. J. Lett.*, 2022, **931**, L4.
57 Y. Yarnall and R. L. Hudson, *Icarus*, 2022, **373**, 114799.
58 R. Luna, G. Molpeceres, J. Ortigoso, M. Á. Satorre, M. Domingo and B. Maté, *Astron. Astrophys.*, 2018, **617**, 116.
59 R. Luna, C. Millán, M. Domingo, C. Santonja and M. Á. Satorre, *Astrophys. J.*, 2022, **935**, 134.
60 J. B. Bossa, K. Isokoski, M. S. de Valois and H. Linnartz, *Astron. Astrophys.*, 2012, **545**, A82.
61 K. Isokoski, J. B. Bossa, T. Triemstra and H. Linnartz, *Phys. Chem. Chem. Phys.*, 2014, **16**, 3456.
62 A. V. Ivlev, B. M. Giuliano, Z. Juhász, P. Herczku, B. Sulik, D. V. Mifsud, S. T. S. Kovács, K. K. Rahul, R. Rácz, S. Biri, I. Rajta, I. Vajda, N. J. Mason, S. Ioppolo and P. Caselli, *Astrophys. J.*, 2023, **944**, 181.